

JGR Atmospheres

RESEARCH ARTICLE

10.1029/2019JD031482

Key Points:

- The variations of the quasi 16-day waves and their response to SSWs are revealed using an extensive
- The rapidly reduced eastward winds during major SSWs are associated with the enhancement of the westward-propagating quasi 16-day waves
- The quasi 16-day waves with Wavenumbers 1 and 2 contribute the formation of the displaced vortex and the split vortex, respectively

Correspondence to:

Y. Gong & S. Zhang, yun.gong@whu.edu.cn; zsd@whu.edu.cn

Citation:

Gong, Y., Wang, H., Ma, Z., Zhang, S., Zhou, Q., Huang, C., & Huang, K. (2019). A statistical analysis of the propagating quasi 16-day waves at high latitudes and their response to sudden stratospheric warmings from 2005 to 2018. *Journal of Geophysical Research: Atmospheres*, 124, 12,617–12 630. https://doi.org/10.1029/2019JD031482

Received 6 AUG 2019 Accepted 15 NOV 2019 Accepted article online 20 NOV 2019 Published online 5 DEC 2019

A Statistical Analysis of the Propagating Quasi 16-Day Waves at High Latitudes and Their Response to Sudden Stratospheric Warmings From 2005 to 2018

Yun Gong^{1,2} D, Hongling Wang^{1,2}, Zheng Ma^{1,2} D, Shaodong Zhang^{1,2,3} D, Qihou Zhou⁴ D, Chunming Huang^{1,2} D, and Kaiming Huang^{1,2} D

¹School of Electronic Information, Wuhan University, Wuhan, China, ²Key Laboratory of Geospace Environment and Geodesy, Ministry of Education, Wuhan, China, ³State Key Laboratory of Information Engineering in Surveying, Mapping and Remote Sensing, Wuhan University, Wuhan, China, ⁴Electrical and Computer Engineering Department, Miami University, Oxford, Ohio, USA

Abstract This study presents an analysis of the long-term variations of four propagating quasi 16-day waves with Wavenumbers 1 and 2 and investigates their association with sudden stratospheric warming (SSW) events. The study is based on the data obtained from Aura Microwave Limb Sounder satellite and Modern-Era Retrospective Analysis for Research and Applications-2 reanalysis data in the period from 2004 to 2018. Strong quasi 16-day waves are found in the winter hemisphere. The propagating waves with Wavenumber 1 are prominent in the Northern Hemisphere and eastward-propagating waves are dominant in the Southern Hemisphere. By analyzing 14 SSW events, we found that the westward-propagating quasi 16-day waves increase rapidly around the onset dates of the major SSWs, which is likely associated with the quickly reduced mean eastward background winds. Based on analysis of geopotential height, Ertel potential vorticity and Eliassen-Palm flux, the propagating quasi 16-day waves with Wavenumbers 1 and 2, (mainly from westward-propagating components) contribute to the formation of the vortex displaced and vortex split SSWs, respectively.

1. Introduction

Planetary waves (PWs) are large-scale atmospheric waves that affect the atmospheric structure and circulation. The periods of PWs are generally 2 to 20 days. Many studies have revealed that PWs are generally excited in the lower atmosphere and propagate upward to the stratosphere and the mesosphere (Day & Mitchell, 2010; Dickinson, 1968; Forbes et al., 1995; Salby, 1981). Among these PWs, the quasi 16-day wave, with periods of 12–20 days, was first observed by Kingsley et al. (1978) using meteor wind data over Sheffield (53°N, 2°W). Since then, studies of the quasi 16-day wave have been carried out extensively (Espy & Witt, 1996; Forbes et al., 1995; Luo, Manson, Meek, Thayaparan, et al., 2002; Manson et al., 2004; Mitchell et al., 1999; Pancheva et al., 2009; Pancheva & Mitchell, 2004).

Salby (1981) reported that the quasi 16-day wave is a westward-propagating normal Rossby mode with zonal Wavenumber 1. Using data obtained from a medium frequency radar in the period from 1980 to 1996 at Saskatoon (52°N, 107°W), Luo et al. (2000) investigated the quasi 16-day wave in the mesosphere and lower thermosphere. Their observations indicated that the quasi 16-day wave prevails in winter and reaches its maximum amplitude at around 60 km. Shankar et al. (2010) investigated the vertical amplitude structure of the quasi 16-day wave using the mesospheric temperature and neutral wind measurements. Their results revealed that the large quasi 16-day wave amplitudes occur at 88–92 km. Wang et al. (2010) studied the characteristics of the high-latitude quasi 16-day wave in the troposphere and lower stratosphere using radiosonde observations at three Alaskan stations. They found that strong quasi 16-day waves exist in the regions around the tropopause and the winter polar night jet. Huang et al. (2017) reported that the quasi 16-day wave has a significant impact on the magnitude and height of the tropospheric jet at middle latitudes.

Seasonal variation of the quasi 16-day wave has been widely investigated in recent years (Day & Mitchell, 2010; Shankar et al., 2010). Alexander and Shepherd (2010) found that the quasi 16-day wave is dominant throughout winter hemispheres in the polar lower stratosphere. Day et al. (2011) stated that the quasi 16-day wave has a clear seasonal cycle with the wave amplitude maximizing in winter, based on the data

©2019. American Geophysical Union. All Rights Reserved. obtained from the Microwave Limb Sounder (MLS) on the Aura satellite in the period from 2004 to 2010. McDonald et al. (2011) investigated both eastward and westward-propagating quasi 16-day waves with zonal Wavenumbers 1 and 2. They found that the amplitudes of westward-propagating waves are larger in the winter of the Northern Hemisphere (NH), while eastward-propagating waves dominate in the Southern Hemisphere (SH).

The NH winter is often accompanied by sudden stratospheric warming (SSW) events. This event is characterized by a sharp increment of temperature in the polar stratosphere, which can rise tens of degrees in a few days (Matsuno, 1971). The SSW is suggested to result from the interaction between the vertical propagating PWs and the polar vortex (Andrews et al., 1987; Matsuno, 1971). The SSW event does not only affect the polar atmosphere but also cause strong disturbances in the atmosphere and ionosphere globally (Chau et al., 2012; Goncharenko et al., 2013; Gong et al., 2013, 2016; Gong, Li, et al., 2018; Gong, Ma, et al., 2018; Ma et al., 2017; Manney et al., 2009). Many studies have reported that the SSWs and the quasi 16day waves are associated (Chen et al., 2016; Laskar et al., 2014; Limpasuvan et al., 2004; Pancheva et al., 2008; Shepherd & Tsuda, 2008). Pancheva et al. (2008) found that prior to the 2004 SSW, an upward and westward-propagating quasi 16-day wave is dominant in the stratosphere and mesosphere. Vineeth et al. (2009) used the NCEP/NCAR reanalysis data to analyze the variations of daytime mesopause temperature over an equatorial station during the 2006 SSW. Their study revealed that the quasi 16-day wave is enhanced in the equatorial mesopause temperature prior to the SSW and indicated that the quasi 16-day wave can propagate from the equatorial stratosphere to the North Pole in about 1 month. Scheiben et al. (2014) investigated the characteristics of the quasi 16-day wave in the mesosphere during boreal winter 2011/2012 using ground-based microwave radiometer and satellite water vapor observations. They found decreased quasi 16-day wave activity during the 2012 SSW. However, most of the studies are based on a single SSW event.

There are several types of SSW, and their classification is discussed later. The propagating quasi 16-day waves have different wavenumbers and directions. Therefore, the different quasi 16-day wave modes may have different association with different types of SSWs, which cannot be fully investigated by using a single SSW event. The main purpose of this study is to present a comprehensive study on the relationship between different propagating quasi 16-day wave modes and different types of SSWs based on 14 SSW events. The data processing method is introduced in section 2. Results and discussions of the seasonal, interannual, and altitudinal variations of the quasi 16-day waves are given in section 3. Section 4 presents a statistical analysis between SSWs and the quasi 16-day waves in the NH. Conclusions are summarized in sections 5.

2. Data Analysis

Temperature data measured by the MLS instrument onboard the Aura satellite is used in this study to investigate the variations of the four propagating quasi 16-day waves with Wavenumbers 1 and 2. The Aura satellite is in a sun-synchronous orbit with an inclination of 98° at an altitude of 705 km, which was launched by the National Aeronautics and Space Administration on 15 July 2004. Approximately 3,500 vertical profiles are measured by Aura MLS per day covering the latitudinal range from 82°S to 82°N. More detailed descriptions about the Aura MLS measurements are found in Waters et al. (2006) and Schwartz et al. (2008).

The version 4.2x Level 2 MLS temperature data is used in this study, which started from Day 215 in 2004. The temperature data at 42 pressure levels from 261 to 0.001 hPa (9–97 km) are available for scientific research with a vertical resolution of ~5 km from 261 to 0.01 hPa (Livesey et al., 2017). First of all, the temperature data are selected based on quality standards including the estimated precision (positive), the status value (even), the quality value (>0.2 for the 83 hPa and below; >0.9 at larger pressures of 100 hPa and above) and the convergence (<1.03; Livesey et al., 2017). Then, the selected temperature data are sorted into 32 latitudinal bins in steps of 5° from 80°S to 80°N. In each latitudinal and altitudinal bin, the amplitudes of the propagating quasi 16-day waves with Wavenumbers from -2 to 2 are extracted using a 32-day sliding window with a step of 1 day (John & Kumar, 2016). In each fitting window, we first perform a two-dimensional fast Fourier transform (2DFFT) to obtain a normalized frequency-wave number power spectrum (Huang et al., 2013; John & Kumar, 2016). Figure 1 presents the result of the 2DFFT in a fitting window (the

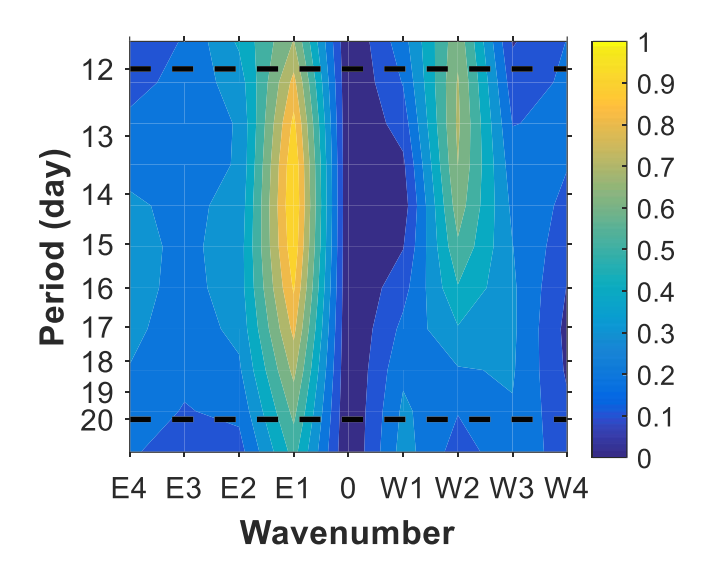


Figure 1. Normalized frequency-wavenumber power spectrum obtained from the MLS temperature in the period from 12 January to 12 February 2008 at 0.05 hPa.

period from 12 January to 12 February 2008 at 0.05 hPa). E1, E2, W1, and W2 represent the eastward-propagating quasi 16-day wave with Wavenumbers 1 and 2 and westward-propagating quasi 16-day wave with Wavenumbers 1 and 2. According to the spectra results, within the periods from 12 to 20 days, the periods correspond to the largest spectra power in E1, E2, W1, and W2 components, are regarded as the quasi 16-day waves in each fitting window. Then, the amplitudes of E1, E2, W1, and W2 components are obtained using the 2DFFT coefficients. The noise level is calculated according to a method described in McDonald et al. (2011). The noise level of E1, E2, W1, and W2 waves are ~0.6, ~0.6, ~0.5, and ~0.5 K, respectively.

The types and onset dates of the SSW events are not defined consistently in previous studies. Kodera et al. (2015) defined the 2010 SSW as a major event while Strahan et al. (2016) identified this event as a minor SSW. Manney et al. (2015) reported that the onset date of the 2015 SSW was 4 January while Gupta and Upadhayaya (2017) stated that the onset date was 26 January. In the present study, the occurrence of the SSW event is determined based on the World Meteorological Organization definition that the zonal mean temperature gradient between 90°N and 60°N becomes positive, and the positive gradient lasts more than 5 days at 10 hPa level. A major SSW is associated with the reversal of

the zonal mean zonal wind at 60°N from eastward to westward at 10 hPa while a minor SSW only has an attenuation of the zonal winds. The onset date of the SSW is defined as the day when the largest temperature gradient occurs. The Modern-Era Retrospective Analysis for Research and Applications-2 (MERRA2) temperature and zonal wind data in the NH from 2005 to 2018 are used in this study to determine the onset dates and the types of SSWs based on the WMO definition. The MERRA2 data are obtained from the National Aeronautics and Space Administration website (https://disc.gsfc.nasa.gov/daac-bin/FTPSubset2.pl). Descriptions of the MERRA2 version of the GEOS-5 AGCM can be found in Molod et al. (2015). Aside from being classified either as major or minor, an SSW event can also be defined as polar vortex displacement (PVD) or polar vortex split (PVS; Charlton & Polvani, 2007). Using the MERRA2 geopotential height data from 2005 to 2018, the SSWs are defined based on vortex-oriented classification. The onset dates and the types of SSW events from 2005 to 2018 are listed in Table 1. Manney and Lawrence (2016) reported a strong stratospheric final warming event occurred in March 2016. The onset dates of the stratospheric final warming events vary from early March to late May. Here, we only focus on the SSW events during the midwinters from December to February.

Table 1	
The Onset Date and Types of SSW Events From 2005 to 20.	18

Year of the SSW events	Date	Туре
2005	24 February	Minor/PVD
2006	22 January	Major/PVD
2007	24 February	Major/PVD
2008	23 February	Major/PVD
2009	23 January	Major/PVS
2010	22 January	Minor/PVD
2011	2 February	Minor/PVD
2012	18 January	Minor/PVD
2013	4 January	Major/PVD
2014	9 February	Minor/PVD
2015	26 January	Minor/PVD
2016	8 February	Minor/PVD
2017	29 January	Minor/PVD
2018	11 February	Major/PVS

3. Long-Term Variations of the Quasi 16-day Wave at High Latitudes

According to previous studies (Day & Mitchell, 2010; John & Kumar, 2016; Luo, Manson, Meek, Meyer, et al., 2002; McDonald et al., 2011), the quasi 16-day waves are dominant at around 60°N/S. In this paper, we focus on the investigation on the propagating quasi 16-day waves with Wavenumbers 1 and 2 at the latitude range from 55° to 65° in both hemispheres. Figure 2 presents the long-term variations of the monthly mean quasi 16-day waves from December 2004 to September 2018 at the latitude range from 55° to 65°. Figures 2a to 2d and 2e to 2h display the time-altitude-amplitude variations of the E1, W1, E2, and W2 waves in the SH and the NH, respectively. The four propagating quasi 16-day waves show similar seasonal variations that approach the maximum amplitudes during each winter in both hemispheres. The largest amplitude reaches up to 8 K. Our results are obtained from a long dataset, which confirms the previous studies that the amplitudes of the quasi 16-day waves are prominent during

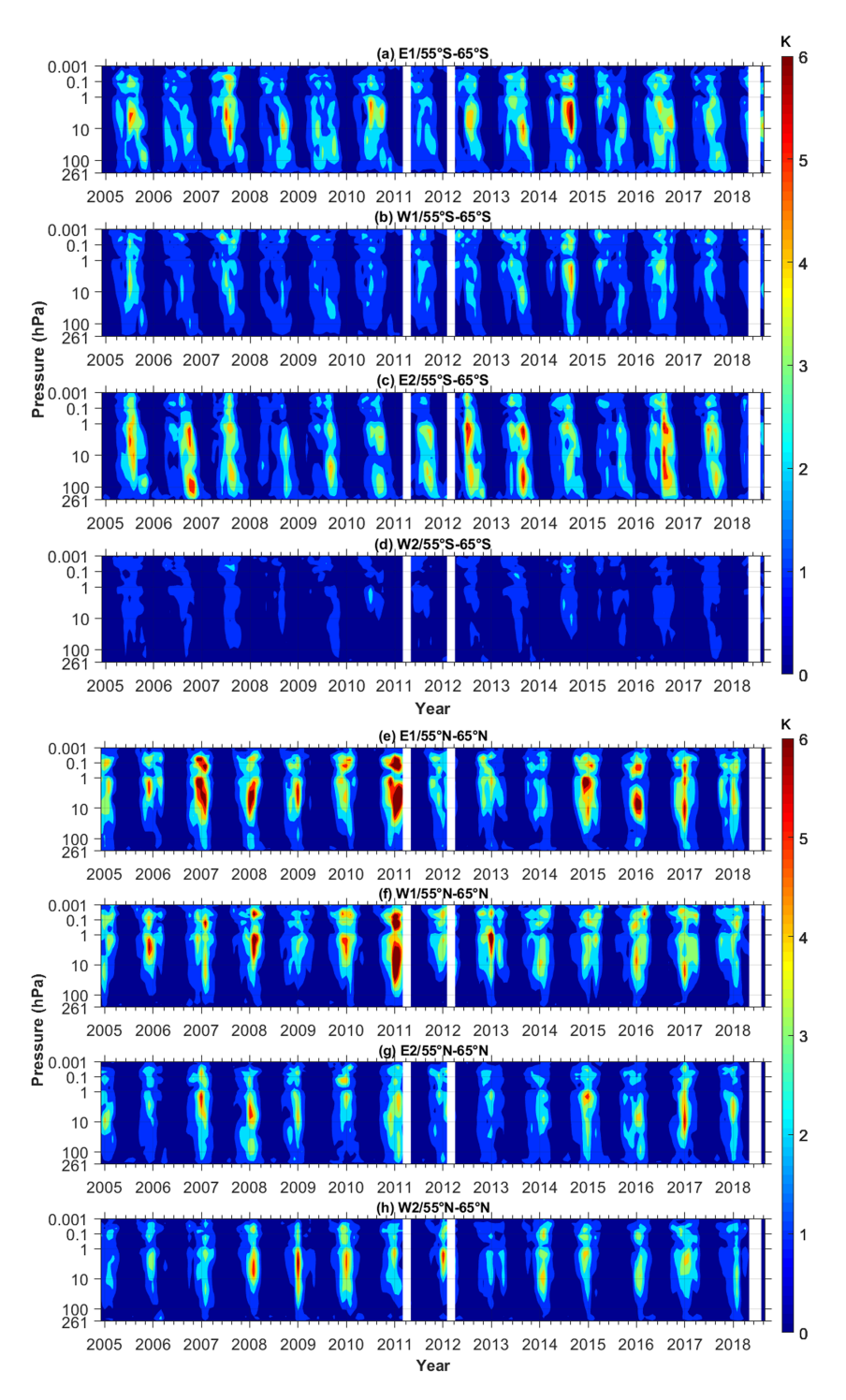


Figure 2. Time-altitude amplitude variations of the monthly mean propagating quasi 16-day waves obtained from Aura/ Microwave Limb Sounder measurements from December 2004 to September 2018 at the latitude range of 55°S to 65°S and 55°N to 65°N. Results (from (a) to (d) and from (e) to (h)) are given for eastward propagation wave with Wavenumber 1 (E1), westward propagation wave with Wavenumber 2 (E2), and westward propagation wave with Wavenumber 2 (W2), respectively.

winter times (Alexander & Shepherd, 2010; Day et al., 2011; John & Kumar, 2016; McDonald et al., 2011).

In the SH, the eastward-propagating waves (Figures 2a and 2c) dominate the westward-propagating waves (Figures 2b and 2d). The W2 wave is nonexistent in the SH since its amplitude is largely below the noise

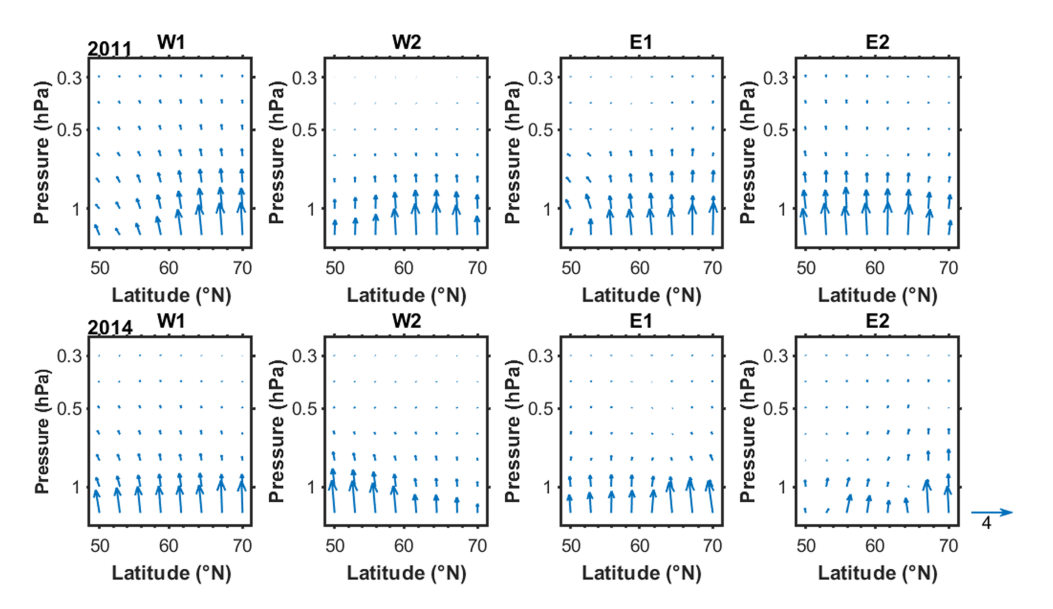


Figure 3. The Eliassen-Palm flux of the eastward/westward (E/W) propagating quasi 16-day waves with Wavenumbers 1 and 2 in the pressure range from 1.3 to 0.3 hPa in January 2011 (top row) and January 2014 (bottom row). The arrow scale denotes 4×10^2 and 4×10^7 kg/s 2 for vertical and meridional components of the Eliassen-Palm flux.

level (~0.5 K). In the NH, the quasi 16-day waves with Wavenumber 1 (Figures 2e and 2f) are much stronger than the waves with Wavenumber 2 (Figures 2g and 2h). Our results are consistent with the MLS study reported by McDonald et al. (2011). However, their results are based on only 4 years of the MLS temperature data (January 2005–December 2008). When comparing the results between the two hemispheres, it can be found that the amplitudes of the westward-propagating modes in the NH are much stronger than in the SH, while the amplitudes of the eastward-propagating modes in both hemispheres are comparable.

As seen from Figure 2, the quasi 16-day waves are strong during winter but not at all interested pressure levels. The amplitudes of the quasi 16-day waves are very weak around 1 hPa (~50 km) that near the stratopause region while the amplitudes above and below this region are strong. Using the Sounding of the Atmosphere using Broadband Emission Radiometry (SABER) temperature measurements in the period from 2003 to 2007, John & Kumar (2016) reported the similar vertical structure of the propagating quasi 16-day waves that the amplitudes are weak around 50 km and strong at ~40 and ~70 km. They suggested that around 50 km (about 1 hPa), the background conditions are not favorable for upward-propagating the quasi 16-day waves (John & Kumar, 2016). However, the quasi 16-day amplitudes above that region are comparable with when they are below 50 km. The Eliassen-Palm (EP) flux has been widely used to study the PW activities (Fritts et al., 1999; Huang et al., 2017; Leroy & Anderson, 2007). The EP flux has two components, which indicates the wave energy propagation in the meridional and vertical directions, respectively. The meridional and vertical components of the EP flux (F) are calculated with the following equations (Andrews et al., 1987; Huang et al., 2017; Iida et al., 2014; Li et al., 2007):

$$F^{(\varphi)} = \rho_0 a\cos\varphi \left(\overline{u_z} \frac{\overline{v'\theta'}}{\overline{\theta_z}} - \overline{u'v'}\right), \tag{1}$$

$$F^{(z)} = \rho_0 a(\cos\varphi) \left\{ \frac{\left[f_0 - (a\cos\varphi)^{-1} (\overline{u}\cos\varphi)_{\varphi} \right] \overline{v'\theta'}}{\overline{\theta_z}} - \overline{u'w'} \right\}, \tag{2}$$

where ρ_0 is the mean density; a is the mean Earth radius; ϕ is the latitude; f_0 is the Coriolis parameter; z is the log-pressure height; u, v, w is the zonal, meridional, and vertical wind, respectively; and θ is the potential temperature. The zonal wind, meridional wind, and temperature data are obtained from the MERRA2 data. The overbars, primes, and subscripts in equations (1) and (2) represent the zonal averages, perturbation

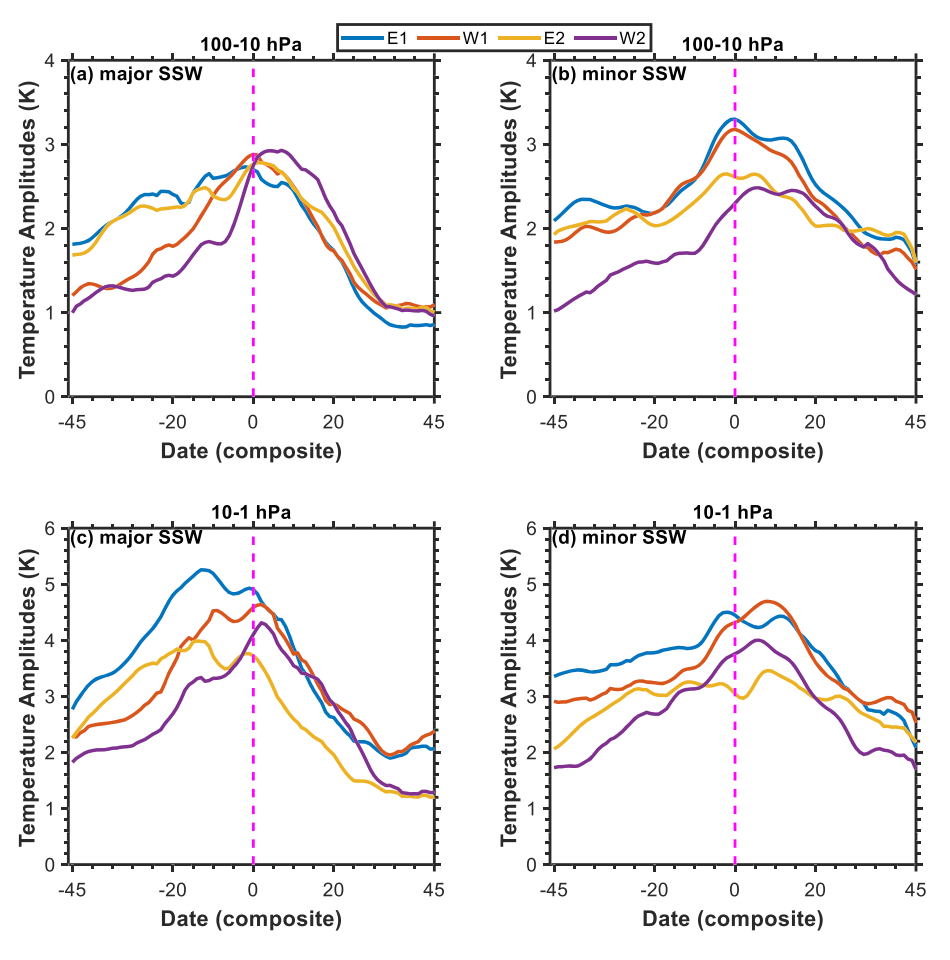


Figure 4. Daily composite variations of the eastward/westward (E/W) propagating quasi 16-day waves with Wavenumbers 1/2 (E1, blue; E2, golden; W1, maroon; W2, purple) during the major sudden stratospheric warmings (SSWs; left column) and minor SSWs (right column). The results are calculated at the latitude range from 55°N to 65°N and in the pressure ranges of 100–10 hPa (top row) and 10–1 hPa (bottom row). The vertical dotted pink lines represent the onset date of SSWs (day 0).

quantities, and the derivatives, respectively. The potential temperature θ is evaluated by the equation expressed by Andrews et al. (1987).

$$\theta = \mathrm{T}(P_{s}/\mathrm{P})^{0.286},\tag{3}$$

where T is the measured temperature, P_s is the standard air pressure of 1,000 hPa, P is the real pressure level of the measured temperature. The EP flux of the propagating quasi 16-day waves during January of 2011 (top panel) and 2014 (bottom panel) in the pressure range from 1.3 to 0.3 hPa are presented in Figure 3. As shown in Figure 2, since the propagating quasi 16-day waves are prominent during the winter of 2011 and are relative weak in the winter of 2014, we only present the results of those 2 years. As seen from Figure 3, the four wave modes all exhibit upward-propagating activities around 1 hPa, which indicates that although it is difficult, the quasi 16-day oscillations can still pass through this region. Ghosh et al. (2019) suggested that the vertical wavelength of the quasi 16-day waves is large enough near the stratopause region, which ensures their propagation to higher altitudes even up to the ionosphere. Nevertheless, the mechanisms of the vertical propagating quasi 16-day waves from the stratosphere to the mesosphere need further investigations.

4. Statistical Analysis of the Quasi 16-day Waves During SSWs

In recent years, studies on the correlation between SSWs and the quasi 16-day wave have attracted more and more attention (Laskar et al., 2014; Pancheva et al., 2008; Scheiben et al., 2014; Vineeth et al., 2010). However, as mentioned in section 1, most of these studies are based on a single SSW event. To further understand the

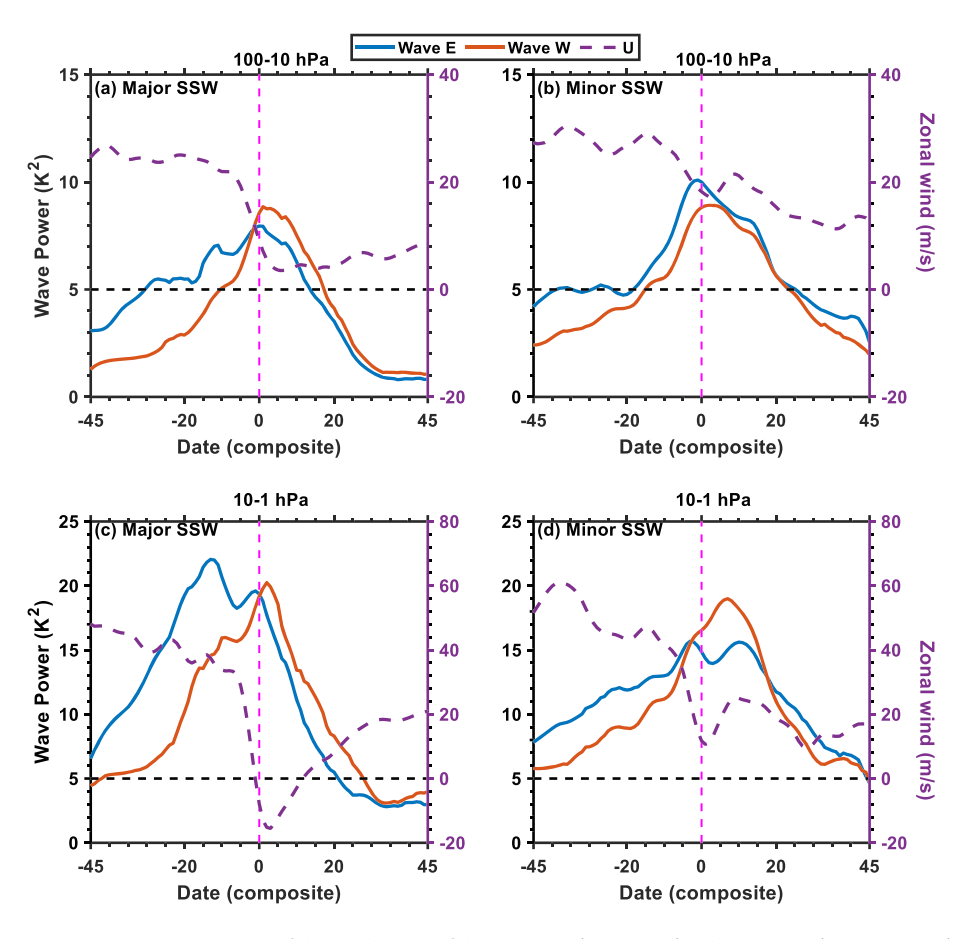


Figure 5. Daily composite variations of the total power of the eastward (blue curve) and westward (maroon curve) propagating quasi 16-day waves and zonal mean wind (purple curve) during major sudden stratospheric warmings (SSWs) (left column) and minor SSWs (right column). The results are calculated at the latitude range from 55°N to 65°N and in the pressure ranges of 100–10 hPa (top row) and 10–1 hPa (bottom row). The vertical dotted pink lines represent the onset date of SSWs (day 0); the horizontal dotted black lines represent the zero wind speed.

variations of the quasi 16-day wave activities during multiple major/minor and PVD/PVS SSWs, a statistical analysis of the four propagating quasi 16-day waves with Wavenumbers 1 and 2 during SSW events from 2005 to 2018 is presented below.

According to the classification shown in Table 1, the daily composite variations of the quasi 16-day waves during the major SSWs (left column) and the minor SSWs (right column) are presented in Figure 4. The results are obtained by averaging the daily quasi 16-day wave amplitudes in the pressure ranges of 100–10 hPa (top row) and 10–1 hPa (bottom row). The dotted pink lines represent the onset date of the SSWs (Day 0). The temporal variations of the four propagating quasi 16-day wave modes are exhibited in the period from 45 days before the SSWs (Day –45) to 45 days after the SSWs (Day 45). Note that the time indexes in the following figures are defined as the last day of the fitting window. As shown in Figure 4, the temporal variations of the W1, W2, and E1 waves are similar. They exhibit a clear enhancement before the commencement of the SSWs, reaching to the maximums around the onset date and then decrease. During the minor SSWs, compared with the other three wave modes, the E2 wave exhibits the least variations.

According to Figure 4, it appears that the eastward/westward-propagating quasi 16-day waves respond differently to different types of SSWs. To investigate the variations of the eastward/westward-propagating quasi 16-day waves during the major/minor SSWs, the wave power of the eastward and westward waves is presented in Figure 5. The total power of the eastward/westward-propagating waves (wave E/W) is the summation of the E1/E2 and W1/W2 wave power, which is calculated using the following equation (Hayashi, 1971):

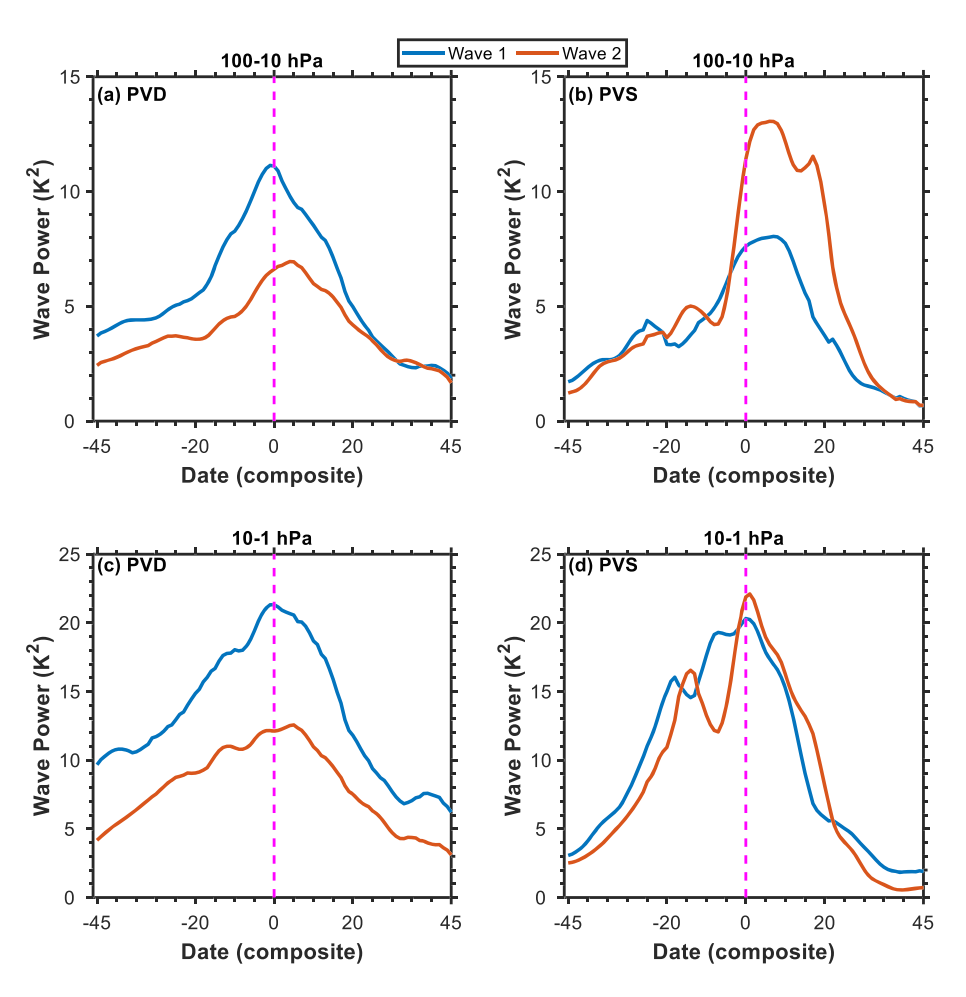


Figure 6. Daily composite variations of the total power of the propagating quasi 16-day waves with Wavenumbers 1 (blue curve) and 2 (maroon curve) during the polar vortex displacement (PVD) SSWs (left column) and polar vortex split (PVS) SSWs (right column). The results are calculated at the latitude range from 55°N to 65°N and in the pressure ranges of 100–10 hPa (top row) and 10–1 hPa (bottom row). The vertical dotted pink lines represent the onset date of SSWs (day 0).

$$P_{s,\pm\omega}(T) = \sum_{s,\pm\omega} \frac{1}{2} R_{s,\pm\omega}^2, \tag{4}$$

where $P_{s,\pm\omega}$ is the wave power of the eastward/westward-propagating quasi 16-day waves; $R_{s,\pm\omega}$ represents the wave amplitude; S is the zonal wavenumber; and ω is the wave frequency. In Figure 5, the purple dashed lines are the zonal mean background wind (eastward positive) obtained from the MERRA2 data. The vertical pink lines and horizontal black lines represent the onset date of the SSWs (Day 0) and the zero wind speed, respectively. As seen from Figure 5, the temporal variations of wave W in both SSW types exhibit a clear enhancement before the commencement of the SSW. Wave W is stronger than wave E in the period from Day 0 to 15 except during the minor SSWs at 100-10 hPa. In the period of Day -10 to 10, wave W quickly increases and then decreases. During the same period, wave E also exhibits the same trend but as not intense as wave W except during the minor SSWs at 100-10 hPa. The variation of waves W and E may be related to the background wind at 10 hPa during the SSWs. The vertical propagation of PWs in the atmosphere is greatly influenced by background winds (Charney & Drazin, 1961; John & Kumar, 2016; McDonald et al., 2011). Charney and Drazin (1961) stated that background winds that are lightly eastward relative to the PW are conducive to their vertical propagation. The zonal phase velocity of quasi 16-day waves with Wavenumbers 1 and 2 at 60°N are approximately 14.7 and 7.3 m/s, respectively. As shown in Figure 5c, the zonal mean background wind decreases from ~33 to ~-16 m/s from Day -5 to 4. During this period, the westward-propagating waves rapidly increases from ~15 to ~20 K². Since the westward-propagating quasi 16-day waves in the lower atmosphere are easier to propagate upward under this background wind

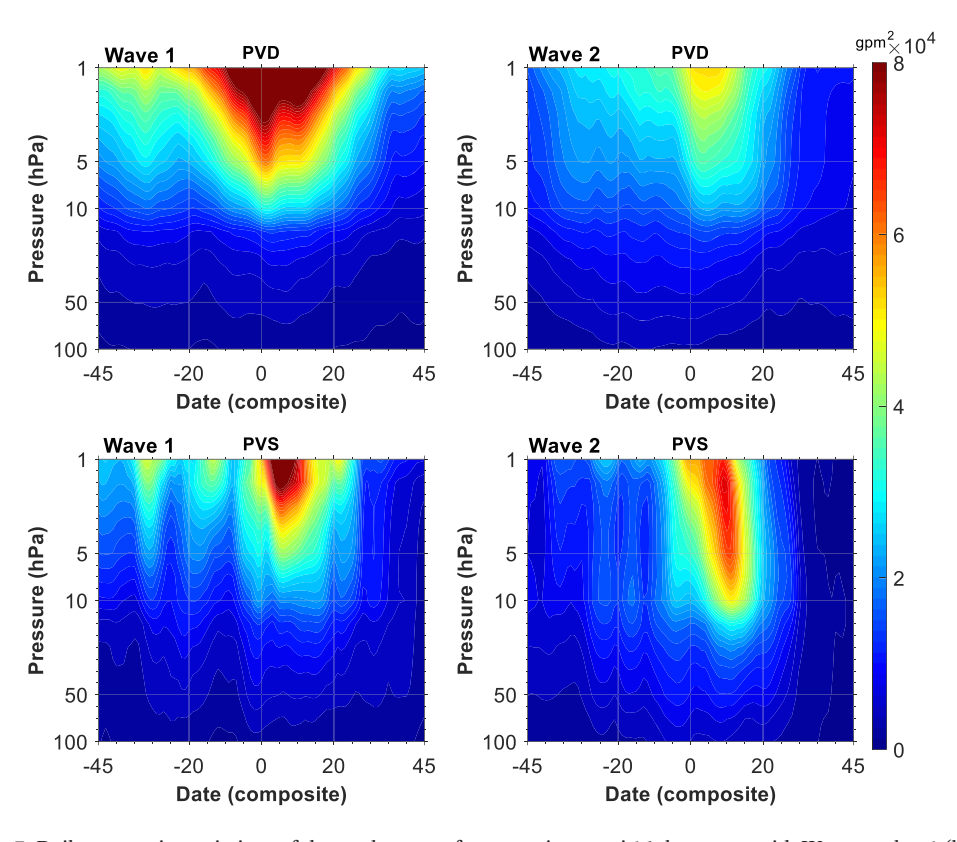


Figure 7. Daily composite variations of the total power of propagating quasi 16-day waves with Wavenumber 1 (left column) and Wavenumber 2 (right column) in the geopotential height during polar vortex displacement (PVD) SSWs (top row) and polar vortex split (PVS) SSWs (bottom row). The results are calculated at the latitude range from 55°N to 65°N and in the pressure ranges of 100–1 hPa. Day 0 represents the onset date of SSWs.

condition, the sharp deceleration of the eastward background wind is likely associated with the quick amplification of the westward-propagating waves.

The PWs with Wavenumbers 1 and 2 are suggested to be associated with PVD and PVS SSWs, respectively (Charlton & Polvani, 2007; Manney et al., 2009). Charlton and Polvani (2007) reported that PVD/PVS SSWs are often associated with large amplitudes of PWs with Wavenumbers 1 and 2. Manney et al. (2009) found large Wave 1 amplitude during the 2006 PVD SSW and intense Wave 2 activity during the 2009 PVS SSW. However, those studies have not identified the wave periods of the PWs. The relationship between the propagating quasi 16-day waves and the PVD/PVS SSWs are rarely reported. In order to understand the relationship, the total wave power of the propagating quasi 16-day waves with Wavenumbers 1 and 2 is exhibited in Figure 6. The total power of the propagating quasi 16-day waves with Wavenumbers 1 and 2 (Waves 1 and 2) is the summation of the E1/W1 and E2/W2 wave energy. As shown in Figures 6a and 6c, Wave 1 dominates Wave 2 in both pressure ranges. Wave 1 in both regions reaches its maximum power around the onset date and then quickly decreases. During the PVS SSWs, the power of Wave 2 at 100-10 hPa rapidly grows, and its maximum reaches to ~13 K² while the maximum of Wave 1 is ~8 K². In the pressure range of 10-1 hPa, Wave 2 exhibits sharp increment and its magnitude increased from 12 to 22 K² in the period from Day -7 to 1. In this pressure range, Wave 2 is also larger than Wave 1 in the period from Day -3 to 21, but the difference is not as significant as it in the pressure range of 100-10 hPa. By examining 12 PVD SSW events, our results indicate that the PVD SSWs have a large impact on the propagating quasi 16-day waves with Wavenumber 1, while the PVS SSWs affect more on the propagating quasi 16-day waves with Wavenumber 2.

On the other hand, the propagating quasi 16-day waves may affect the formation of the polar vortex and contribute to PVD/PVS SSWs. The geopotential height distribution is often used to express the state of the polar vortex, where higher geopotential height value refers to the anticyclones and lower geopotential height value

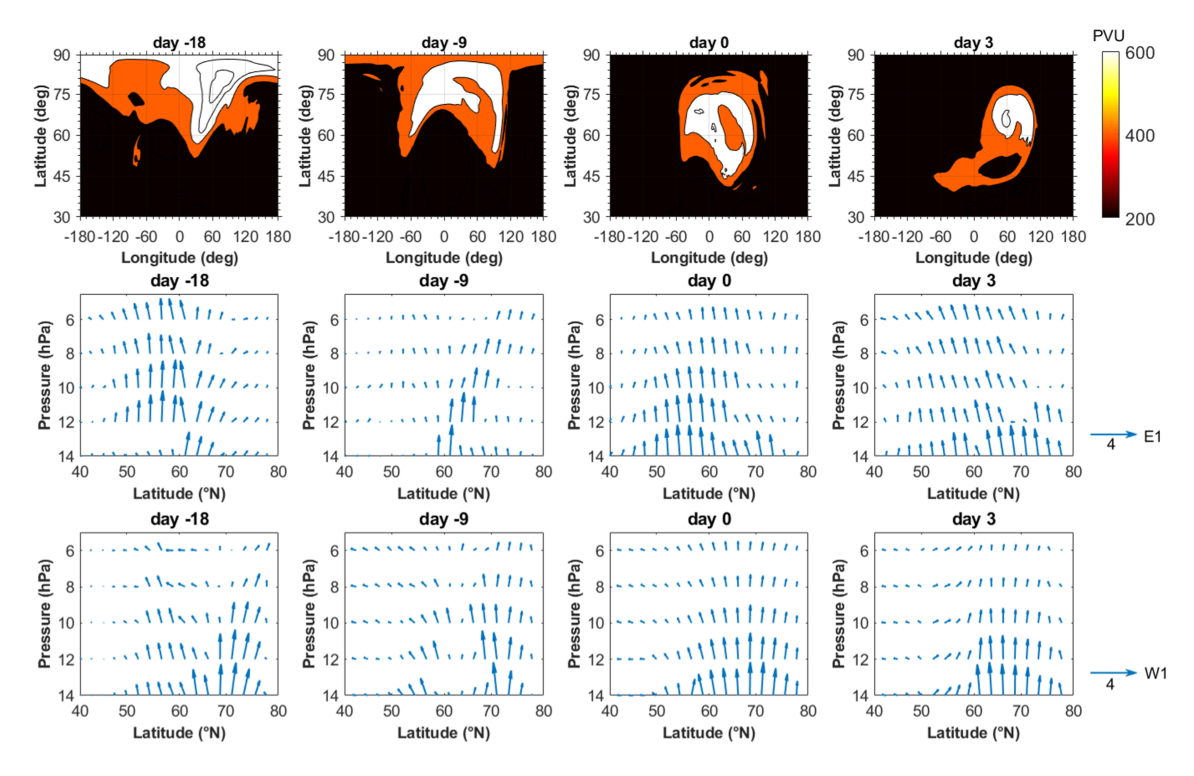


Figure 8. The composite evolutions of the Ertel potential vorticity at 10 hPa (top row) and the Eliassen-Palm flux of the E1 and W1 quasi 16-day waves (middle and bottom row) for days -18, -9, 0, and 3 during polar vortex displacement SSWs. The arrow scale denotes 4×10^2 and 4×10^5 kg/s² for vertical and meridional components of the EP flux. Day 0 represents the onset date of polar vortex displacement sudden stratospheric warmings.

represents the polar vortices. The composite results of the quasi 16-day oscillations in the geopotential height during the PVD/PVS SSWs are presented in Figure 7. The geopotential height data is obtained from the MERRA2 data. The results are computed in the pressure range of 100–1 hPa from 55°N to 65°N. Since the distribution of the geopotential height is closely related to the polar vortices, the variations shown in the geopotential height are indicative of the variations of the polar vortices. As shown in Figure 7, Wave 1 is dominant during the PVD SSWs. During the PVS SSWs, Wave 2 is larger than Wave 1 below about 3 hPa. It indicates that Wave 2 contributes more than Wave 1 in the split polar vortex, although many studies suggested that PWs with Wavenumber 1 has a large contribution in the formation of the split polar vortex. Waves 1 and 2 reach the maximum around the onset dates in PVD SSWs while it takes about 10 more days for those two waves to achieve their maximum in the PVS SSWs.

Aside from the geopotential height, the activity of the Ertel potential vorticity (EPV) also provides the evolution process of the polar vortices (Nash et al., 1996). Matthewman et al. (2009) suggested that the Arctic polar vortex could be identified by the air mass of the high EPV values, corresponding to the lower geopotential height values. Hoppel et al. (2008) stated that major SSW is associated with the advection of low potential vorticity air over the pole near 10 hPa. Using numerical simulations, Scaife and James (2000) investigated the advection of the EPV in the upper stratosphere. Their results revealed that the northward and eastward advection of the low EPV air shaves off a strip of high potential vorticity from the polar vortex. Coy and Pawson (2015) reported that propagating PWs can advect enough low EPV air into the polar region and create strong anticyclones to displace or split the polar vortex. We derived the composite EPV evolutions at 10 hPa during the PVD and PVS SSWs. Note that, the EPV distributions over the polar region are not obvious during minor SSWs. Thus, composite EPV evolutions are only calculated in major SSW events (2007–2008).

Coy et al. (2009) found that the poleward development of the low EPV air is related to the poleward EP flux caused by the PWs. They suggested that the PWs play an important role in the displacement of the SSW. Many studies have used the EP flux to reveal the magnitude and direction of the energy propagation caused by the PWs (Chen & Huang, 2002; Harada et al., 2010; Huang et al., 2017; Koval et al., 2018; Leroy &

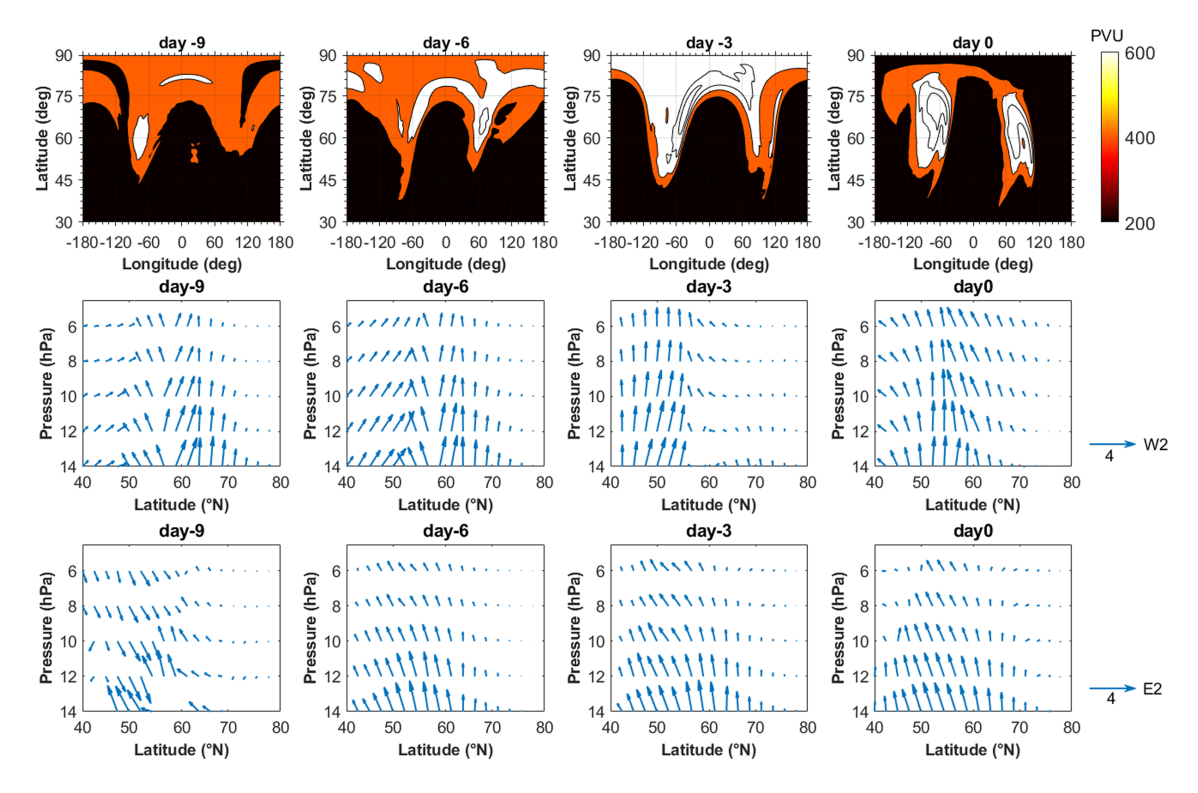


Figure 9. The composite-evolutions of the Ertel potential vorticity at 10 hPa (top row) and the Ertel potential flux of the W2 and E2 quasi 16-day waves (middle and bottom row) for days -9, -6, -3, and 0 during polar vortex split sudden stratospheric warmings. The arrow scale denotes 4×10^2 and 4×10^5 kg/s² for vertical and meridional components of the EP flux. Day 0 represents the onset date of PVS SSWs.

Anderson, 2007; Portafaix et al., 2003). The composite EP flux of the quasi 16-day waves with different wavenumbers at 10 hPa is calculated.

Figure 8 presents the composite result of the EPV evolution (top panel), the EP flux of the E1 (middle panel), and the EP flux of the W1 (bottom panel) during the PVD SSWs. The results of the EP flux of the W2 and E2 are not shown because of their weak association with the PVD SSWs. As shown in Figure 8 (top panel), results of the EPV evolutions are presented in four days (Days -18, -9, 0, and 3), the black shadow denotes the low EPV air, and the white shadow represents the high EPV air. At Day -18 (18 days before the onset date of the SSW), the high EPV air dominates in the polar region, and low EPV air is largely below 60°N. At Day -9, low EPV air becomes important at high latitudes in the longitudinal ranges from 120° to 180° and -180° to -120° . At Day 0, the low EPV air dominates in the polar region, which results in the displacement of the polar vortices from the polar region to lower latitudes. The evolutions of the EPV air at 10 hPa may indicate development of low EPV air (around 180° meridian) from lower latitudes into the polar region. During this period, the polar vortex (indicated by high EPV values) displaces off the pole with a wave-1 pattern. The distribution of EPV is likely associated with the poleward energy transportation as indicated by the EP flux results shown in Figure 8 (middle and bottom panels). The EP flux reveals that the quasi 16-day waves are mainly propagating upward and poleward (at the high latitudes) prior to the onset date of the SSW. The poleward EP flux of the E1 wave is obvious in 60-70°N at Days -18 and -9, while W1 wave provides more poleward energy at higher latitudes (>70°N). This poleward EP flux indicates that the E1 and W1 quasi 16-day waves may contribute to the evolution of the EPV prior to PVD SSWs.

Figure 9 is similar to Figure 8 but for the PVS SSW events. The composite results of the EPV evolution (top panel), the EP flux of the W2 (middle panel), and the EP flux of the E2 (bottom panel) during PVS SSWs are shown at Days -9, -6, -3, and 0. The results of the EP flux of the waves with Wavenumber 1 are not shown because of their weak association with the PVS SSWs. As shown in Figure 9, the low EPV air (black shadows) around 180° meridian is largely below 70°N at Days -9 and -6, and it becomes important in the polar region at Day 0. In addition, the low EPV around 0° meridian also exhibits a poleward development. The evolutions of low EPV around 180° and 0° meridian are likely causing the polar vortex splitting into two parts on Day 0,



when the split SSWs occurred. This process indicates a different poleward development of the EPV during PVS SSWs, where the low EPV air is gradually important in the pole region around 180° and 0° meridians. It reveals a typical wave-2 pattern during the PVS SSWs. As shown in Figure 9 (middle panel), the EP flux of the W2 wave higher than 60°N reveals a strong poleward characteristic at Days -9 and -6. On Day -3, the upward EP flux of the W2 is not strong at higher latitudes but still shows poleward feature around 50°N. As seen from Figure 9 (middle and bottom panels), the overall contribution of the poleward transportation from E2 wave is not as strong as the W2 wave, but it has contributions on Day -3. Our results indicate that the evolution of EPV during PVS SSWs is likely associated with the poleward EP flux of the W2 and E2 waves, and the W2 wave plays a major role. Results shown in Figures 8 and 9 reveal that the propagating quasi 16-day wave with Wavenumber 1 may contribute to the vortex displacements, and W2 and E2 waves are likely associated with the evolution of the EPV during vortex split events.

5. Conclusions

The seasonal and interannual variations of four propagating quasi 16-day waves with Wavenumbers 1 and 2 are analyzed in this study. The analysis is based on temperature data measured by the MLS onboard the Aura satellite from 2004 to 2018. Aside from the variations of the quasi 16-day waves, the relation between the four quasi 16-day modes and four types of SSWs (major/minor, PVD/PVS) in the period from 2005 to 2018 are investigated for the first time.

Based on the large dataset, our results reveal that the four propagating quasi 16-day waves are strong in the winter hemisphere. The wave amplitudes surpass 4 K during most of the wintertime. In the NH winter, the quasi 16-day waves with Wavenumber 1 are the most prominent while the eastward-propagating quasi 16-day waves dominate the SH winter. The quasi 16-day waves in the NH are generally larger than in the SH.

The variations of the W1, W2, and E1 waves are similar during the SSWs. Their amplitudes increase before the commencement of the SSWs and reach to the maximum around the onset dates. The westward-propagating quasi 16-day waves are quickly amplified around the onset dates of the major SSWs. Wave 1 is dominant in the PVD SSW in the pressure range of 100–1 hPa, while the power of Wave 2 has a sharp enhancement about 5 days before the onset dates of the PVS SSWs. According to the results of the quasi 16-day wave in the geopotential height, it appears that the quasi 16-day waves with Wavenumber 1 are associated more with the PVD SSWs while the quasi 16-day waves with Wavenumber 2 are linked more with the PVS SSWs. The results of the EPV evolution and EP flux indicate that the quasi 16-day waves with Wavenumber 1 is associated with the formation of the displaced vortex while quasi 16-day waves with Wavenumber 2 (mainly W2) contribute on the split of the polar vortex. By analyzing 14 SSW events in the period of 2005 to 2018, our results reveal that the propagating quasi 16-day waves are strongly associated with the SSWs and they contribute to the displacement and split polar vortices. Nevertheless, the underlined mechanisms between the variations of the quasi 16-day waves and the SSWs are not well understood. In future studies, numerical simulations are needed to further investigate the association between the quasi 16-day waves and the SSWs.

Acknowledgments

We would like to thank the anonymous referees for their helpful comments on the paper. We are grateful to the MERRA data team for access to the data on https://disc.gsfc.nasa.gov/daac-bin/ FTPSubset2.pl and the Jet Propulsion Laboratory (JPL) EOS MLS science team for access to the EOS Aura MLS data on https://disc.gsfc.nasa.gov/ datasets?page=1&keywords=ML2T_ 004. The study is supported by the National Key R&D program of China (2018YFC1407305), the National Natural Science Foundation of China (through grants 41574142 and 41531070), and National Science Foundation grant :AGS-1744033

References

Alexander, S. P., & Shepherd, M. G. (2010). Planetary wave activity in the polar lower stratosphere. *Atmospheric Chemistry and Physics*, 10(2), 707–718. https://doi.org/10.5194/acp-10-707-2010

Andrews, D. G., Holton, J. R., & Leovy, C. B. (1987). Middle atmosphere dynamics. London: Academic Press.

Charlton, A. J., & Polvani, L. M. (2007). A new look at stratospheric sudden warmings. Part I: Climatology and modeling benchmarks. Journal of Climate, 20(3), 449–469. https://doi.org/10.1175/jcli3996.1

Charney, J. G., & Drazin, P. G. (1961). Propagation of planetary-scale disturbances from the lower into the upper atmosphere. *Journal of Geophysical Research*, 66(1), 83–109. https://doi.org/10.1029/JZ066i001p00083

Chau, J. L., Goncharenko, L. P., Fejer, B. G., & Liu, H. L. (2012). Equatorial and low latitude ionospheric effects during sudden stratospheric warming events. Space Science Reviews, 168(1-4), 385–417. https://doi.org/10.1007/s11214-011-9797-5

Chen, G., Wu, C., Zhang, S., Ning, B., Huang, X., Zhong, D., et al. (2016). Midlatitude ionospheric responses to the 2013 SSW under high solar activity. *Journal of Geophysical Research: Space Physics*, 121, 790–803. https://doi.org/10.1002/2015JA021980

Chen, W., & Huang, R. (2002). The propagation and transport effect of planetary waves in the northern hemisphere winter. Advances in Atmospheric Sciences, 19(6), 1113–1126. https://doi.org/10.1007/s00376-002-0069-x

Coy, L., Eckermann, S., & Hoppel, K. (2009). Planetary wave breaking and tropospheric forcing as seen in the stratospheric sudden warming of 2006. *Journal of the Atmospheric Sciences*, 66(2), 495–507. https://doi.org/10.1175/2008JAS2784.1

Coy, L., & Pawson, S. (2015). The major stratospheric sudden warming of January 2013: Analyses and forecasts in the geos-5 data assimilation system. Monthly Weather Review, 143(2), 491–510. https://doi.org/10.1175/mwr-d-14-00023.1

- Day, K. A., Hibbins, R. E., & Mitchell, N. J. (2011). Aura MLS observations of the westward-propagatings=1, 16-day planetary wave in the stratosphere, mesosphere and lower thermosphere. *Atmospheric Chemistry and Physics*, 11(9), 4149–4161. https://doi.org/10.5194/acp-11-4149-2011
- Day, K. A., & Mitchell, N. J. (2010). The 16-day wave in the Arctic and Antarctic mesosphere and lower thermosphere. Atmospheric Chemistry and Physics, 10(3), 1461–1472. https://doi.org/10.5194/acp-10-1461-2010
- Dickinson, R. E. (1968). Planetary Rossby waves propagating vertically through weak westerly wind wave guides. *Journal of the Atmospheric Sciences*, 25(6), 984–1002. https://doi.org/10.1175/1520-0469(1968)025<0984:PRWPVT>2.0.CO;2
- Espy, P. J., & Witt, G. (1996). Observation of a quasi 16-day oscillation in the polar summer mesospheric temperature. Geophysical Research Letters, 23(10), 1071–1074. https://doi.org/10.1029/96GL01068
- Forbes, J. M., Hagan, M. E., Miyahara, S., Vial, F., Manson, A. H., Meek, C. E., & Portnyagin, Y. I. (1995). Quasi 16-day oscillation in the mesosphere and lower thermosphere. *Journal of Geophysical Research*, 100(D5), 9149–9163. https://doi.org/10.1029/ 94ID02157
- Fritts, D. C., Isler, J. R., Lieberman, R. S., Burrage, M. D., Marsh, D. R., Nakamura, N., et al. (1999). Two-day wave structure and mean flow interactions observed by radar and high resolution Doppler imager. *Journal of Geophysical Research*, 104(D4), 3953–3969. https://doi.org/10.1029/1998JD200024
- Ghosh, P., Ramkumar, T. K., Patra, A. K., Sharma, S., & Pavan Chaitanya, P. (2019). Vertical coupling from the lower atmosphere to the ionosphere: Observations inferred from Indian MST radar, GPS radiosonde, ionosonde, magnetometer, OLR (NOAA), and SABER/TIMED instrument over Gadanki. *Journal of Geophysical Research: Space Physics*, 124(1), 489–503. https://doi.org/10.1029/ 2018JA025897
- Goncharenko, L. P., Hsu, V. W., Brum, C. G. M., Zhang, S. R., & Fentzke, J. T. (2013). Wave signatures in the midlatitude ionosphere during a sudden stratospheric warming of January 2010. *Journal of Geophysical Research: Space Physics*, 118, 472–487. https://doi.org/10.1029/ 2012JA018251
- Gong, Y., Li, C., Ma, Z., Zhang, S., Zhou, Q., Huang, C., et al. (2018). Study of the quasi-5-day wave in the MLT region by a meteor radar chain. *Journal of Geophysical Research: Atmospheres*, 123(17), 9474–9487. https://doi.org/10.1029/2018JD029355
- Gong, Y., Ma, Z., Lv, X., Zhang, S., Zhou, Q., Aponte, N., & Sulzer, M. (2018). A study on the quarterdiurnal tide in the thermosphere at Arecibo during the February 2016 sudden stratospheric warming event. Geophysical Research Letters, 45(23), 13,142–13,149. https://doi. org/10.1029/2018GL080422
- Gong, Y., Zhou, Q., & Zhang, S. (2013). Atmospheric tides in the low-latitude E and F regions and their responses to a sudden stratospheric warming event in January 2010. Journal of Geophysical Research: Space Physics, 118, 7913–7927. https://doi.org/10.1002/2013JA019248
- Gong, Y., Zhou, Q., Zhang, S., Aponte, N., & Sulzer, M. (2016). An incoherent scatter radar study of the midnight temperature maximum that occurred at Arecibo during a sudden stratospheric warming event in January 2010. *Journal of Geophysical Research: Space Physics*, 121, 5571–5578. https://doi.org/10.1002/2016JA022439
- Gupta, S., & Upadhayaya, A. K. (2017). Morphology of ionospheric F2 region variability associated with sudden stratospheric warmings. Journal of Geophysical Research: Space Physics, 122, 7798–7826. https://doi.org/10.1002/2017JA024059
- Harada, Y., Goto, A., Hasegawa, H., Fujikawa, N., Naoe, H., & Hirooka, T. (2010). A major stratospheric sudden warming event in January 2009. Journal of the Atmospheric Sciences, 67(6), 2052–2069. https://doi.org/10.1175/2009JAS3320.1
- Hayashi, Y. (1971). A generalized method of resolving disturbances into progressive and retrogressive waves by space Fourier and time cross-spectral analysis. *Journal of the Meteorological Society of Japan*, 49(2), 125–128. https://doi.org/10.2151/jmsj1965.49.2_125
- Hoppel, K. W., Baker, N. L., Coy, L., Eckermann, S. D., McCormack, J. P., Nedoluha, G. E., & Siskind, D. E. (2008). Assimilation of stratospheric and mesospheric temperatures from MLS and SABER into a global NWP model. Atmospheric Chemistry and Physics, 8(20), 6103–6116. https://doi.org/10.5194/acp-8-6103-2008
- Huang, C., Zhang, S., Chen, G., Zhang, S., & Huang, K. (2017). Planetary wave characteristics in the lower atmosphere over Xianghe (117.00°E, 39.77°N), China, revealed by the Beijing MST radar and MERRA data. *Journal of Geophysical Research: Atmospheres*, 122, 9745–9758. https://doi.org/10.1002/2017JD027029
- Huang, Y. Y., Zhang, S. D., Yi, F., Huang, C. M., Huang, K. M., Gan, Q., & Gong, Y. (2013). Global climatological variability of quasi-two-day waves revealed by TIMED/SABER observations. *Annales Geophysicae*, 31(6), 1061–1075. https://doi.org/10.5194/angeo-31-1061-2013
- Iida, C., Hirooka, T., & Eguchi, N. (2014). Circulation changes in the stratosphere and mesosphere during the stratospheric sudden warming event in January 2009. Journal of Geophysical Research: Atmospheres, 119, 7104–7115. https://doi.org/10.1002/ 2013JD021252
- John, S. R., & Kumar, K. K. (2016). Global normal mode planetary wave activity: A study using timed/saber observations from the stratosphere to the mesosphere-lower thermosphere. Climate Dynamics, 47(12), 3863–3881. https://doi.org/10.1007/s00382-016-3046-2
- Kingsley, S. P., Muller, H. G., Nelson, L., & Scholefield, A. (1978). Meteor winds over Sheffield (53°N, 2°W). Journal of Atmospheric and Terrestrial Physics, 40(8), 917–922. https://doi.org/10.1016/0021-9169(78)90143-5
- Kodera, K., Mukougawa, H., Maury, P., Ueda, M., & Claud, C. (2015). Absorbing and reflecting sudden stratospheric warming events and their relationship with tropospheric circulation. *Journal of Geophysical Research: Atmospheres*, 121, 80–94. https://doi.org/10.1002/ 2015JD023359
- Koval, A. V., Gavrilov, N. M., Pogoreltsev, A. I., & Shevchuk, N. O. (2018). Influence of solar activity on penetration of traveling planetary-scale waves from the troposphere into the thermosphere. *Journal of Geophysical Research: Space Physics*, 123, 6888–6903. https://doi.org/10.1029/2018JA025680
- Laskar, F. I., Pallamraju, D., & Veenadhari, B. (2014). Vertical coupling of atmospheres: Dependence on strength of sudden stratospheric warming and solar activity. Earth Planets & Space, 66(1), 1–10. https://doi.org/10.1186/1880-5981-66-94
- Leroy, S. S., & Anderson, J. G. (2007). Estimating Eliassen-Palm flux using COSMIC radio occultation. Geophysical Research Letters, 34, L10810. https://doi.org/10.1029/2006GL028263
- Li, Q., Graf, H.-F., & Giorgetta, M. A. (2007). Stationary planetary wave propagation in Northern Hemisphere winter climatological analysis of the refractive index. Atmospheric Chemistry and Physics, 7(1), 183–200. https://doi.org/10.5194/acp-7-183-2007
- Limpasuvan, V., Thompson, D. W. J., & Hartmann, D. L. (2004). The life cycle of the northern hemisphere sudden stratospheric warmings. Journal of Climate, 17(13), 2584–2596. https://doi.org/10.1175/1520-0442(2004)017<2584:TLCOTN>2.0.CO;2
- Livesey, N. J., Read, W. G., Wagner, P. A., Froidevaux, L., Lambert, A., Manney, G. L., et al. (2017). EOS MLS version 4.2x Level 2 data quality and description document, Tech. Rep. Pasadena, CA: Jet Propulsion Laboratory, California Institute of Technology. https://mls.jpl.nasa.gov/data/v4-2_data_quality_document.pdf



- Luo, Y., Manson, A. H., Meek, C. E., Meyer, C. K., Burrage, M. D., Fritts, D. C., et al. (2002). The 16-day planetary waves: Multi-mf radar observations from the arctic to equator and comparisons with the HRDI measurements and the GSWM modelling results. Annales Geophysicae, 20(5), 691–709. https://doi.org/10.5194/angeo-20-691-2002
- Luo, Y., Manson, A. H., Meek, C. E., Meyer, C. K., & Forbes, J. M. (2000). The quasi 16-day oscillations in the mesosphere and lower thermosphere at saskatoon (52°N, 107°W), 1980-1996. *Journal of Geophysical Research Atmospheres*, 105(D2), 2125–2138. https://doi.org/10.1029/1999JD900979
- Luo, Y., Manson, A. H., Meek, C. E., Thayaparan, T., Macdougall, J., & Hocking, W. K. (2002). The 16-day wave in the mesosphere and lower thermosphere: Simultaneous observations at Saskatoon (52°N, 107°W) and London (43°N, 81°W), Canada. *Journal of Atmospheric and Solar-Terrestrial Physics*, 64(8-11), 1287–1307. https://doi.org/10.1016/S1364-6826(02)00042-1
- Ma, Z., Gong, Y., Zhang, S., Zhou, Q., Huang, C., Huang, K., et al. (2017). Responses of quasi 2 day waves in the MLT region to the 2013 SSW revealed by a meteor radar chain. *Geophysical Research Letters*, 44, 9142–9150. https://doi.org/10.1002/2017GL074597
- Manney, G. L., & Lawrence, Z. D. (2016). The major stratospheric final warming in 2016: Dispersal of vortex air and termination of arctic chemical ozone loss. *Atmospheric Chemistry and Physics*, 16, 15,371–15,396. https://doi.org/10.5194/acp-16-15371-2016
- Manney, G. L., Lawrence, Z. D., Santee, M. L., Read, W. G., Livesey, N. J., Lambert, A., et al. (2015). A minor sudden stratospheric warming with a major impact: Transport and polar processing in the 2014/2015 arctic winter. *Geophysical Research Letters*, 42, 7808–7816. https://doi.org/10.1002/2015GL065864
- Manney, G. L., Schwartz, M. J., Krüger, K., Santee, M. L., Pawson, S., & Lee, J. N. (2009). Aura Microwave Limb Sounder observations of dynamics and transport during the record-breaking 2009 Arctic stratospheric major warming. *Geophysical Research Letters*, 36, L12815. https://doi.org/10.1029/2009GL038586
- Manson, A. H., Meek, C. E., Chshyolkova, T., Avery, S. K., Thorsen, D., Macdougall, J. W., et al. (2004). Longitudinal and latitudinal variations in dynamic characteristics of the MLT (70-95 km): A study involving the CUJO network. *Annales Geophysicae*, 22(2), 347–365. https://doi.org/10.5194/angeo-22-347-2004
- Matsuno, T. (1971). A dynamical model of the stratospheric sudden warming. *Journal of the Atmospheric Sciences*, 28(8), 1479–1494. https://doi.org/10.1175/1520-0469(1971)028<1479:ADMOTS>2.0.CO;2
- Matthewman, N. J., Esler, J. G., Charlton-Perez, A. J., & Polvani, L. M. (2009). A new look at stratospheric sudden warmings. Part iii: Polar vortex evolution and vertical structure. *Journal of Climate*, 22(6), 1566–1585. https://doi.org/10.1175/2008JCLI2365.1
- McDonald, A. J., Hibbins, R. E., & Jarvis, M. J. (2011). Properties of the quasi 16 day wave derived from EOS MLS observations. *Journal of Geophysical Research*, 116, D06112. https://doi.org/10.1029/2010JD014719
- Mitchell, N. J., Middleton, H. R., Beard, A. G., Williams, P. J. S., & Muller, H. G. (1999). The 16-day planetary wave in the mesosphere and lower thermosphere. *Annales Geophysicae*, 17(11), 1447–1456. https://doi.org/10.1007/s00585-999-1447-9
- Molod, A., Takacs, L., Suarez, M., & Bacmeister, J. (2015). Development of the GEOS-5 atmospheric general circulation model: Evolution from MERRA to MERRA2. Geoscientific Model Development, 8(5), 1339–1356. https://doi.org/10.5194/gmd-8-1339-2015
- Nash, E. R., Newman, P. A., Rosenfield, J. E., & Schoeberl, M. R. (1996). An objective determination of the polar vortex using Ertel's potential vorticity. *Journal of Geophysical Research*, 101(D5), 9471–9478. https://doi.org/10.1029/96JD00066
- Pancheva, D., Mukhtarov, P., Mitchell, N. J., Merzlyakov, E., Smith, A. K., Andonov, B., et al. (2008). Planetary waves in coupling the stratosphere and mesosphere during the major stratospheric warming in 2003/2004. *Journal of Geophysical Research*, 113, D12105. https://doi.org/10.1029/2007JD009011
- Pancheva, D., Mukhtarov, R., Andonov, B., Mitchell, N. J., & Forbes, J. M. (2009). Planetary waves observed by timed/saber in coupling the stratosphere-mesosphere-lower thermosphere during the winter of 2003/2004: Part 1-Comparison with the UKMO temperature results. Journal of Atmospheric and Solar-Terrestrial Physics, 71(1), 75–87. https://doi.org/10.1016/j.jastp.2008.09.027
- Pancheva, D. V., & Mitchell, N. J. (2004). Planetary waves and variability of the semidiurnal tide in the mesosphere and lower thermosphere over Esrange (68°N, 21°E) during winter. *Journal of Geophysical Research Space Physics*, 109(A8), A08307. https://doi.org/10.1029/2004JA010433
- Portafaix, T., Morel, B., Bencherif, H., Baldy, S., Godin-Beekmann, S., & Hauchecorne, A. (2003). Fine-scale study of a thick stratospheric ozone lamina at the edge of the southern subtropical barrier. *Journal of Geophysical Research*, 108(D6), 4196. https://doi.org/10.1029/2002/D002741
- Salby, M. L. (1981). Rossby normal modes in nonuniform background configurations. Part I: Simple fields. *Journal of the Atmospheric Sciences*, 38(9), 1803–1826. https://doi.org/10.1175/1520-0469(1981)038<1803:RNMINB>2.0.CO;2
- Scaife, A. A., & James, I. N. (2000). Response of the stratosphere to interannual variability of tropospheric planetary waves. Quarterly Journal of the Royal Meteorological Society, 126(562), 275–297. https://doi.org/10.1002/qj.49712656214
- Scheiben, D., Tschanz, B., Hocke, K., Kämpfer, N., Ka, S., & Oh, J. J. (2014). The quasi 16-day wave in mesospheric water vapor during boreal winter 2011/2012. Atmospheric Chemistry and Physics, 14(13), 6511–6522. https://doi.org/10.5194/acp-14-6511-2014
- Schwartz, M. J., Lambert, A., Manney, G. L., Read, W. G., & Livesey, N. J. (2008). Validation of the Aura Microwave Limb Sounder temperature and geopotential height measurements. *Journal of Geophysical Research*, 113(D15), D15S11. https://doi.org/10.1029/2007JD008783
- Shankar, D. S., Kishore, K. K., Veena, S. B., & Geetha, R. (2010). Simultaneous observation of quasi 16 day wave in the mesospheric winds and temperature over low latitudes with the SKiYMET radar. *Radio Science*, 45, RS6014. https://doi.org/10.1029/2009RS004300
- Shepherd, M. G., & Tsuda, T. (2008). Large-scale planetary disturbances in stratospheric temperature at high-latitudes in the southern summer hemisphere. *Atmospheric Chemistry and Physics*, 8(4), 16,409–16,444. https://doi.org/10.5194/acpd-8-16409-2008
- Strahan, S. E., Douglass, A. R., & Steenrod, S. D. (2016). Chemical and dynamical impacts of stratospheric sudden warmings on arctic ozone variability. *Journal of Geophysical Research: Atmospheres*, 121, 11,836–11,851. https://doi.org/10.1002/2016JD025128
- Vineeth, C., Pant, T. K., Kumar, K. K., Ramkumar, G., & Sridharan, R. (2009). Signatures of low latitude-high latitude coupling in the tropical mlt region during sudden stratospheric warming. Geophysical Research Letters, 36, L20104. https://doi.org/10.1029/ 2009GL040375
- Vineeth, C., Pant, T. K., Kumar, K. K., & Sumod, S. G. (2010). Tropical connection to the polar stratospheric sudden warming through quasi 16-day planetary wave. *Annales Geophysicae*, 28(11), 2007–2013. https://doi.org/10.5194/angeo-28-2007-2010
- Wang, R., Zhang, S. D., & Fan, Y. I. (2010). Radiosonde observations of high-latitude planetary waves in the lower atmosphere. *Science China Earth Sciences*, 53(6), 919–932. https://doi.org/10.1007/s11430-010-0069-0
- Waters, J. W., Froidevaux, L., Harwood, R. S., Jarnot, R. F., Pickett, H. M., & Read, W. G. (2006). The Earth Observing System Microwave Limb Sounder (EOS MLS) on the Aura satellite. *IEEE transactions on geoscience and remote sensing*, 44(5), 1075–1092. https://doi.org/ 10.1109/TGRS.2006.873771